SIMULATION ANALYSES OF A NON-KINEMATICAL CONICAL ROLL BENDING PROCESS WITH CONICAL ROLLS

Zhengkun Feng [a], Henri Champliaud [b], Thien-My Dao[c]

Department of Mechanical Engineering, École de technologie supérieure, University of Quebec,
1100 Notre-Dame Street West, Montreal, Quebec, H3C 1K3, Canada

[a]feng.zhengkun@etsmtl.ca, [b]henri.champliaud@etsmtl.ca, [c] thien-my.dao@etsmtl.ca

ABSTRACT

In order to reuse the existing conical rolls of the kinematical conical roll bending process, attachments are added in the non-kinematical conical roll bending process to reduce the velocity of the top edge of the plate. In contrast with a kinematical conical roll bending machine, the driving outer rolls of a non-kinematical conical roll bending machine are allowed to slide on the zone close to the top edge of the plate due to the friction between the attachments and the plate. Therefore, the appropriate velocity obtained at the top edge of the plate makes it possible to roll the plate using the kinematical conical roll bending process. This paper deals with the simulation analyses of the non-kinematical multi-pass conical roll bending process based on the finite element method. A well bent cone was obtained compared with the ideal cone and the numerical simulation results show that the bent cone depends on the static and dynamic friction coefficients for a geometrical configuration with an appropriate span of the outer rolls.

Keywords: conical roll bending, three-dimensional, Finite element method, Simulation

NOMENCLATURE

d Span between the outer rolls
h Real height of the desired cone
H Whole height of the desired cone
l_i Available length of the inner roll
l_o Available length of the outer rolls
L_i Whole length of the inner roll
L_o Whole length of the outer rolls
r Top radius of the desired cone
r_{pi} Inside radius of the plate
r_i Top radius of the inner roll
r_o Top radius of the outer rolls
R Bottom radius of the desired cone
R_{po} Outside radius of the plate
R_i Bottom radius of the inner roll
R_o Bottom radius of the outer rolls
t Plate thickness
ϕ Angle of the desired cone
θ_{len} Angular length of the plate
θ_{xy} Angle with XY plane
θ_{xz} Angle with XZ plane
θ_{yz} Angle with YZ plane

1. INTRODUCTION

Large and long tubular sections used in industries are usually assembled with several segments and high geometrical quality of bent cones is required, such as the manufacturing of a crown of Francis turbines (Figure 1). For the purpose of satisfying the hydraulic profile (Fig. 1a), a crown is conventionally manufactured by foundry process which takes unexpected long time so the process becomes very expensive. An alternative process, which is capable of achieving an approximate hydraulic profile and accelerating the manufacture, was proposed (Marroquin 2002). With this process, a crown can be obtained by assembling several cone segments, for example, three cones of different size (Fig. 1b).

Both continuous conical roll bending and continuous cylindrical roll bending use usually three-roll or four-roll bending machines. Intensive research on the process of four-roll bending machines was undertaken for understanding the bending mechanism by Hua and his colleagues (Hua and Lin 1999a, Hua et al., 1994, Hua, Baines, and Cole 1995, Hua, Sansome, and Baines 1995, Hua et al., 1997, Hua, Baines, and Cole 1999, Hua and Lin 1999b, Lin and Hua 2000). Such bending machines have the advantage in eliminating the planar zones close to the leading and trailing edges of the plate. This advantage is significant if the plate is thin in cylindrical roll bending process. However, it is not efficient for conical bending (Hua and Lin 1999a, Roggendorff and Haeusler 1979), especially if the plate to be bent is thick. In addition, the process is more complex than that of the three-roll bending machines, the pre-bending for eliminating the planar zones needs to position the plate repeatedly. Although analyses of pyramidal three-roll bending process in cylindrical roll bending as two-dimensional modeling can be found in literature (Roggendorff and Haeusler 1979, Yang, Mori, Osakada 1994, Yang and Shima 1988, Ramamurti, Rao, Sriram 1972, Bassett and Johnson 1966, Gandhi and Raval 2008), it is necessary to apply more complete theory to a three-dimensional model of conical roll bending process.

With the fast evolution of computer science and technology, powerful computational technology makes such applications possible. For example, the finite element method is widely used in solid mechanics and commercial software is easily accessible for efficient analyses through numerical simulations, such as the well-known commercial software ANSYS/LS-DYNA. Three-dimensional modeling based on finite element method can be found recently in literature, such as the modeling and simulation of kinematical conical roll bending process (Zeng, Liu, and Champliaud 2008) and non-kinematical conical roll bending process with conical rolls (Feng et al. 2007, Feng, Champliaud, and Dao 2008).

This paper deals with the simulation analyses of the non-kinematical multi-pass conical roll bending process with conical rolls based on the finite element method. The remaining sections of this paper are organized as follows: Section 2 presents the operational sequences of the symmetrical pyramidal three-roll bending process; Section 3 describes the geometrical configurations of the three-dimensional model; Section 4 discusses the model based on finite element method. Section 5 presents the numerical simulation results with discussion, and finally, conclusions will be drawn.

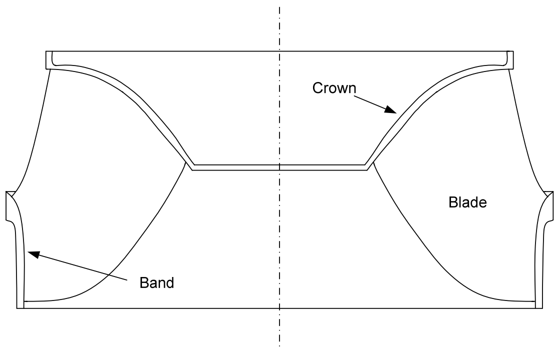

(a)

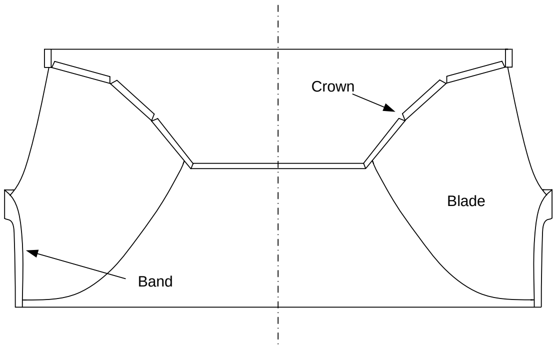

(b)

Figure 1: A crown with components of a Francis turbine (from Ref. 1 with modification)

2. OPERATIONAL SEQUENCES

Figure 2 illustrates the front view of the geometrical configuration of a simplified model of a symmetrical pyramidal three-roll bending machine. The model consists essentially of one plate, one inner roll and two outer rolls. The two identical outer rolls with a constant distance between their axes and in a symmetrical position related to the inner roll are driving rolls while the inner roll is able to move in the vertical direction in order to press down the plate to reach a desired curvature. The dot lines represent the initial positions of the plate and the inner roll while the continuous lines represent the deformed plate and the final position of the inner roll. The four small vertical cylinders are used as guides to keep the plate from moving away from the bending machine. The two small horizontal semi-cylinders are used as attachments (see zoom without the guiding cylinders). The distances between the plate/attachment contact lines (the contact lines between the plate and the attachments) and the outer contact lines (the contact lines between the plate and the outer rolls) are exactly the thickness of the plate. During the roll bending process, the inner roll presses the plate down to a desired position at point B, where the inner contact line (the contact line between the inner roll and the plate) passes and in the meanwhile, the plate is driven by the rotation of the two outer rolls. The curvature of the deformed plate at point B is supposed to be the desired curvature of the desired cone. It decreases progressively from point B to point A and point C, respectively. The zones of the plate between the leading edge and the outer contact line (point A) at the beginning and between the trailing edge and the inner contact line (point C) at the end of the process will never pass under the inner roll, and will stay planar (In fact, it is not strictly planar due to the deformation produced by the pressing of the inner roll on the inner contact line).

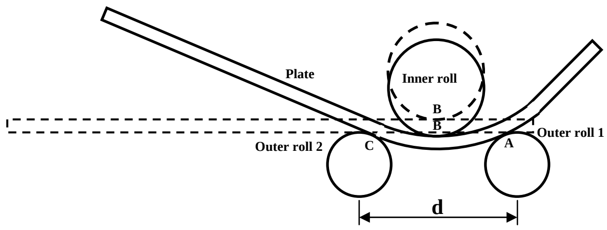

Figure 2: Front view of a symmetrical pyramidal three-roll bending machine

3. GEOMETRICAL CONFIGURATION

Figure 3 illustrates the initial geometrical configurations of the non-kinematical conical bending model. The process is determined by the final position of the desired cone with some parameters provided by customers and engineers, such as the top and bottom radii, the height of the desired cone and the thickness of the plate by customers and the top and bottom radii of the rolls and the span of the outer rolls (the distance between the axes of the outer rolls) by engineers. With these parameters, the other necessary geometrical parameters of the model are calculated in the following section. Since the axes of the two outer rolls can only rotate around their axes during the roll bending process, their initial positions, which are also their final positions, will be determined first, then the initial position of the plate, and finally, those of the inner roll, will be determined.

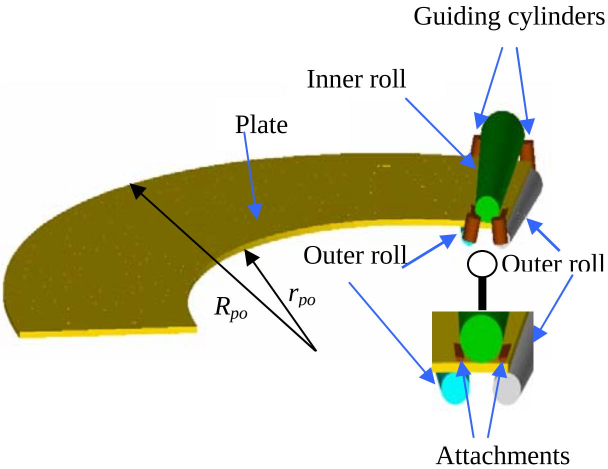

Figure 3: Initial positions of the components of a pyramidal three-roll bending machine in the non-kinematical roll bending process with conical rolls

3.1. Position of the outer rolls

The bottom center of the cone is chosen as the origin of the global Cartesian system, where axis Z coincides with the axis of the desired cone (Fig. 4). The geometry of the final cone determines the position of the outer rolls, where the cone angle ϕ is determined by its height, its top and bottom radii, as follows:

$$\phi = \tan^{-1}\left(\frac{R-r}{H}\right) \tag{1}$$

The position of the apex of the outline of the cone locates at P(0, 0, R/tanϕ) and the angle between the axis of an outer roll and the outer contact lines is:

$$\beta = \sin^{-1}\left(\frac{(R_o - r_o)\sin\phi}{R-r}\right) \tag{2}$$

Adding the two previous angles yields the angle between the cone axis and the axis of each outer roll as follows:

$$\alpha = \phi + \beta \tag{3}$$

The available length of the outer rolls, which are truncated cones, is:

$$l_o = L_o\left(1 - \frac{r_o}{R_o}\right) \tag{4}$$

where L_o is the whole length of the outer rolls (the shape of non-truncated cones)

$$L_o = \frac{R_o}{\tan\beta} \tag{5}$$

The angles between the outer rolls and the XY, YZ, XZ planes can be obtained from the following equations:

$$\theta_{xyo} = \sin^{-1}\left(\frac{d\sin\beta}{2(L_o\sin\alpha\sin\beta + R\sin\beta - R_o\sin\phi)}\right) \tag{6}$$

$$\theta_{yzo} = \tan^{-1}\left(\tan\alpha\cos\theta_{xyo}\right) \tag{7}$$

$$\theta_{xzo} = \tan^{-1}\left(\tan\alpha\sin\theta_{xyo}\right) \tag{8}$$

The apexes of the outer rolls locate at points $P_{o1}(x_{o1}, y_{o1}, z_{o1})$ and $P_{o2}(x_{o2}, y_{o2}, z_{o2})$, respectively, where

$$x_{o1} = -x_{o2} = \left(\frac{R_o}{\sin\beta} - \frac{R}{\sin\phi}\right)\sin\phi\sin\theta_{xyo} \tag{9}$$

$$y_{o1} = y_{o2} = \left(\frac{R_o}{\sin\beta} - \frac{R}{\sin\phi}\right)\sin\phi\cos\theta_{xyo} \tag{10}$$

$$z_{o1} = z_{o2} = H + \left(\frac{R_o}{\sin\beta} - \frac{R}{\sin\phi}\right)\cos\phi \tag{11}$$

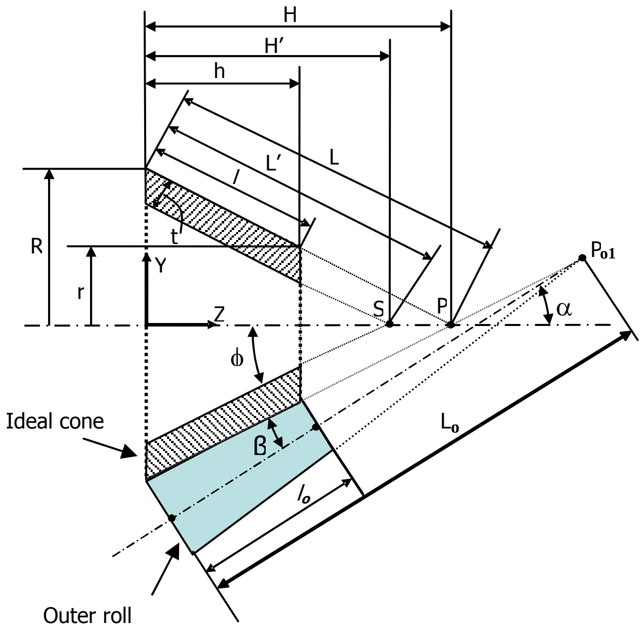

Figure 4: Positions of the desired cone and the conical outer rolls

3.2. Initial position of the plate

As the plate to be bent is determined by the desired cone or the ideal cone, the outside and inside radii of the plate (Fig. 3) are determined by the cone angle, the top and bottom radii of the cone and its height as follows:

$$R_{po} = \frac{R}{\sin\phi} \tag{12}$$

$$r_{po} = \frac{H-h}{\cos\phi} \tag{13}$$

The angles of the plane of the initial plate with the XY, XZ and YZ planes are:

$$\theta_{xyp} = \theta_{xzp} = 0 \tag{14}$$

$$\theta_{yzp} = \tan^{-1}\left(\tan(\alpha-\beta)\cos\theta_{xyo}\right) \tag{15}$$

The center of the plate locates at point (0, 0.5t$\cos\theta_{xyo}$, H-0.5t$\sin\theta_{xyo}$) and the angular length of the plate is:

$$\theta_{len} = \frac{2\pi R}{R_{po}} \tag{16}$$

3.3. Position of the inner roll

The initial and final positions of the inner roll, the initial position of the plate and the final position of the bent cone are illustrated in Figure 5. The position of the inner apex of the cone locates at point S(0, 0, H') (Fig. 4), where H'=H-t/sinϕ. The angle of the inner roll with the outline of the desired cone is:

$$\beta' = \sin^{-1}\left(\frac{(R_i - r_i)\sin\beta}{(R_o - r_o)}\right) \tag{17}$$

So the angle between the inner roll axis and the cone axis becomes:

$$\alpha' = \phi - \beta' \tag{18}$$

The available length of the inner roll, which is also a truncated cone, is:

$$l_i = L_i\left(1 - \frac{r_i}{R_i}\right) \tag{19}$$

where L_i is the whole length of the inner roll (the shape of a non-truncated cone)

$$L_i = \frac{R_i}{\tan\beta'} \tag{20}$$

The initial angles of the inner roll with the XY, XZ and YZ planes can be obtained from the following equations:

$$\theta_{xyi0} = \theta_{xzi0} = 0 \tag{21}$$

$$\theta_{yzi0} = \theta_{yzp} - \beta' \tag{22}$$

The initial position of the apex of the inner roll locates at point $P_{i0}(0, y_{i0}, z_{i0})$, where

$$\begin{aligned} y_{i0} = &(L_i\cos(\theta_{yzp}-\beta') - R_i\sin(\theta_{yzp}-\beta') \\ &- t\sin\theta_{yzp} - H')\tan\theta_{yzp} \end{aligned} \tag{23}$$

$$\begin{aligned} z_{i0} = &L_i\cos(\theta_{yzp}-\beta') \\ &- R_i\cos(\theta_{yzp}-\beta') - t\sin\theta_{yzp} \end{aligned} \tag{24}$$

Similarly, the final angles of the inner roll with the XY, XZ and YZ planes can be obtained from the following equations:

$$\theta_{xyi} = \theta_{xzi} = 0 \tag{25}$$

$$\theta_{yzi} = \phi - \beta' \tag{26}$$

The final position of the apex of the inner roll locates at point $P_i(0, y_i, z_i)$, where

$$\begin{aligned} y_i = &(L_i\cos(\phi-\beta') \\ &- R_i\sin(\phi-\beta') - t\sin\phi - H')\tan\phi \end{aligned} \tag{27}$$

$$z_i = L_i\cos(\phi-\beta') - R_i\cos(\phi-\beta') - t\sin\phi \tag{28}$$

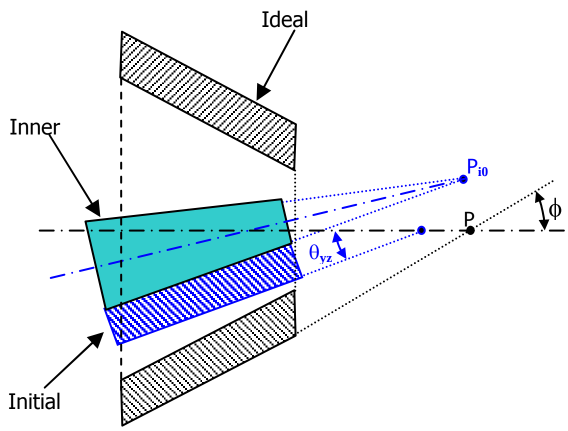

Figure 5: Initial positions of the inner roll and the plate and the final position of the plate (the bent cone)

4. FINITE ELEMENT MODELLING

Although finding a model capable of accurately to represent the roll bending process is the objective of this research, the following assumptions were applied for the purposes of computational efficiency:

- For the plate, the material is considered isotropic, with bilinear elastoplastic deformation behaviour (see the stress–strain curve in Figure 6), with constant properties for the elastic modulus E, the yield stress σ_Y and the tangent modulus E_T.
- The static and dynamic friction coefficients are constant on the plate/attachment contact lines and on the outer contact lines, zero on the inner contact line.
- The rolls, the attachment and the guiding cylinders are rigid bodies.
- The weight of the plate is not considered.

During the roll bending process, a downward force is applied on the inner contact line through the inner roll, and the neighbor zone of the plate encounters an elastic deformation (section OA) (Fig. 6) at first, followed by plastic deformation (section AB). This zone shifts from the leading edge to the trailing edge of the plate as the two outer rolls drive the plate to move forwards and the deformed zone attempts to return to its original state due to the springback. However, the plate stays finally at its equilibrium position at point D. The modeling and the numerical simulations are performed with ANSYS/LS-DYNA based on finite element method with explicit scheme. The finite element model uses the four-node shell elements of type shell163 to descritize the space domain. The governing equations of a deformable body in motion can be described as follows:

$$\sigma_{ij,j} + \rho f_i = \rho \ddot{x}_i \tag{29}$$

with the following boundary conditions:

$$\sigma_{ij} n_i = t_i(t) \tag{30}$$

The discretization of equations (29) and equations (30) based on the finite element method yields the following matrix equations:

$$\mathbf{M}\ddot{\mathbf{x}}(t) + \mathbf{F}(\mathbf{x}, \dot{\mathbf{x}}) - \mathbf{P}(\mathbf{x}, t) = 0 \tag{31}$$

The following explicit time integrations are applied to these semi-discretized equations to find sequentially the solutions (Hallquist 2005).

When the central difference time integration is applied to equations (31), the acceleration at time n can be obtained as

$$\ddot{\mathbf{x}}^n = \mathbf{M}^{-1}[\mathbf{P}^n - \mathbf{F}^n] \tag{32}$$

The velocities at time n+1/2 and the coordinates at time n+1 are explicitly updated as

$$\dot{\mathbf{x}}^{n+1/2} = \dot{\mathbf{x}}^{n-1/2} + \Delta t^n \ddot{\mathbf{x}}^n \tag{33}$$

$$\mathbf{x}^{n+1} = \mathbf{x}^n + \Delta t^{n+1/2} \dot{\mathbf{x}}^{n+1/2} \tag{34}$$

This approach has advantage for modeling structural dynamic system with large displacements and small deformations.

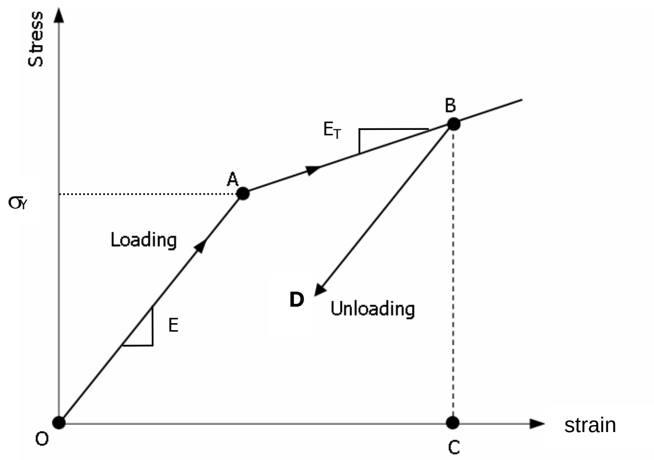

Figure 6: Simplified relation between the stress and strain of the plate

5. NUMERICAL SIMULATIONS

The numerical simulations were performed with a model based on finite element method described in the previous section. The material of the plate was assumed to be ASTM A36 steel. The shell elements (shell163 in ANSYS/LS-DYNA) were used to discretize the plate by 10 elements in the radial direction and 40 elements in the circumferential direction (Fig. 7). The other components of the roll bending machine were modeled with rigid four-node shell elements in order to save computational time. The geometrical parameters of the model and the properties of the ASTM A36 steel at the forming temperature of 400 ^oC are listed in Table 1. The radius ratio between the top and bottom of the rolls was 0.65 which is greater than 0.6 of the kinematical conical roll bending process, while the static and dynamic friction coefficients on the outer contact lines were 0.6 and 0.3, respectively. The process was a multi-pass with three passes. For a configuration as determined in section 2 with the parameters provided in Table 1, the final shape of the cone depended on the span of the outer rolls d, the static and dynamic friction coefficients F_{sa} and F_{da} on the plate/attachment contact lines. For this case, a well closed cone with a small gap between the leading and trailing edges was obtained when d was 0.992 m, F_{sa} and F_{da} were 0.8 and 0.4, respectively (Fig. 8). To verify the quality of the bent cone, firstly, the helical distortion of the top and bottom edges and the gap between the leading and trailing edges of the bent cone is analyzed with the parameters illustrated in Figure 9, where d1 is the distance between points B_1

(the intersection point of the bottom edge with the trailing edge of the final cone) and B_2 (the intersection point of the bottom edge with the leading edge of the final cone), similarly, d2 is the distance between points S_1 (the intersection point of the top edge with the trailing edge of the final cone) and S_2 (the intersection point of the top edge with the leading edge of the final cone). d3 and d4 are used for the measurement of distortion in the circumferential direction at the top and the bottom of the cone, respectively. d5 and d6 are used for the measurement of the helical distortion in the corresponding perpendicular direction (the direction parallel to the leading edge). The deviations of the helical distortion and the gap of the final cone are shown in Table 2. The helical distortion is as very small as 1 cm and the gap is also small. Secondly, the verification was performed with the comparison of the bent cone to an ideal cone. A fitted cone was obtained from the bent cone (Feng et al. 2007) (Fig. 10) and compared with the ideal cone as given in Table 1 (Fig. 11). The deviations of the top and bottom radii, the height and the angle of the fitted cone from the ideal cone were calculated as follows:

$$r_{err} = abs\left(\frac{r_f - r}{r}\right) \tag{35}$$

$$R_{err} = abs\left(\frac{R_f - R}{R}\right) \tag{36}$$

$$h_{err} = abs\left(\frac{h_f - h}{h}\right) \tag{37}$$

$$\phi_{err} = abs\left(\frac{\phi_f - \phi}{\phi}\right) \tag{38}$$

where r_{err}, R_{err}, h_{err} and ϕ_{err} are the deviations of the top and bottom radii, the height and the angle of the fitted cone from the ideal cone, r_f, R_f, h_f and ϕ_f are the top and bottom radii, the height and the angle of the fitted cone. These deviations are shown in Table 3 with the largest value of less than 8% occurring on the top radius of the fitted cone.

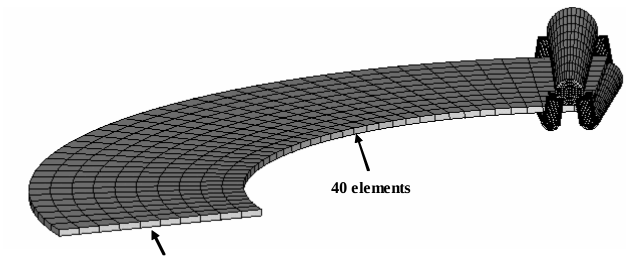

Figure 7: Mesh of the model with shell elements

Table 1: Geometrical parameters of the bending model and the material properties of the plate

Geometrical parameters:	
Cone:	
Height (m)	2.5
Top radius (m)	1.5
Bottom radius (m)	3.0
Inner roll:	
Bottom radius (m)	0.375
Radius ratio	0.65
Outer roll:	
Bottom radius (m)	0.25
Radius ratio	0.65
Material properties of steel ASTM A36 (400^{o}C):	
Elastic modulus (GPa)	166
Yield stress (MPa)	562
Tangent modulus (GPa)	1.6
Poisson's ratio	0.3
Density (kg/m^3)	7850

Table 2: Deviations of the helical distortion and the gap of the final cone

d3(cm)	d4 (cm)	d5 (cm)	d6 (cm)
12.4	12.5	1.1	0.9

Table 3: Deviations of the fitted cone from the ideal cone

r_{err} (%)	R_{err} (%)	h_{err} (%)	ϕ_{err} (%)
7.8	4.56	0.0556	0.0058

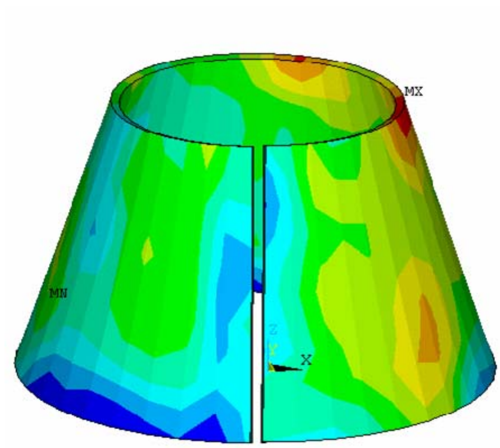

Figure 8: A bent cone obtained from non-kinematical conical roll bending with conical rolls

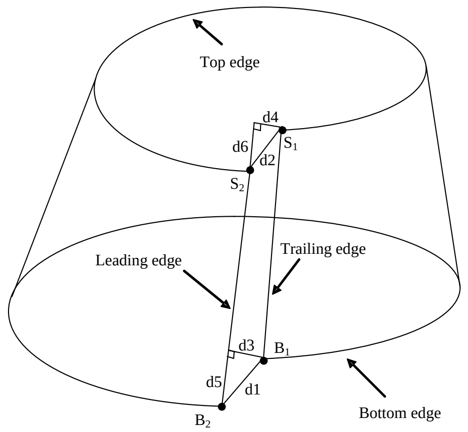

Figure 9: Parameters for determining the helical distortion of the final cone

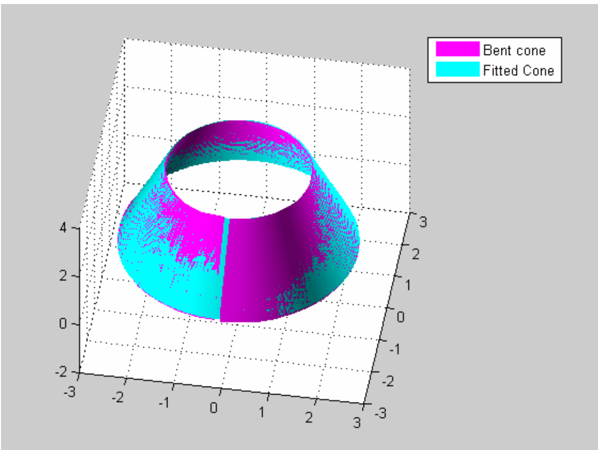

Figure 10: Fitted cone obtained from the bent cone

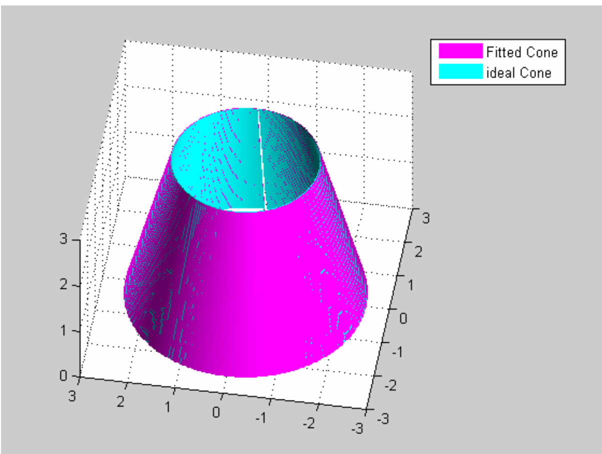

Figure 11: Fitted cone compared with the ideal cone

6. CONCLUSIONS

Continuous non-kinematical conical roll bending process with conical rolls has the advantage of reusing the existing conical rolls of kinematical conical roll bending process. For a determined geometrical configuration, the velocity ratio between the top and bottom edges of the plate is determined by the ratio of the top and bottom radii of the rolls together with the friction at the plate attachment contact. Therefore, the bent cone depends on the static and dynamic friction coefficients on the plate/attachment contact lines and the span between the two outer rolls. When using the existing inner and outer rolls with a determined ratio between the top and bottom radii, the desired closed cone can be obtained by adjusting the static and dynamic friction coefficients at the plate/attachment contact lines and the span between the two outer rolls. This process is less expensive and more adaptive than the kinematical roll bending process due to the possibility of the reuse of the existing rolls. However, these roll bending machines are not capable of eliminating the planar portions close to the leading and trailing edges of the plate as the kinematical roll bending process of pyramidal three-roll bending machines. Eliminating these planar zones by repeating the roll bending process after welding the closed cone remains one of the goals to be pursued in the future.

ACKNOWLEDGMENTS

The authors express their thanks to the Natural Sciences and Engineering Research Council (NSERC) of Canada and General Electric Canada for their financial support for this research.

REFERENCES

Bassett, M.B., Johnson, W., 1966. The bending of plate using a three roll pyramid type plate bending machine. *Journal of Strain Analysis for Engineering Design*, I(5), 398-414.

Feng, Z., Champliaud, H., Dao, T.M., 2008. Modeling and Simulation of Non-Kinematic Conical Roll Bending Process with Conical Rolls. Submitted to *Journal of Manufacturing Science and Technology*.

Feng, Z., Champliaud, H., Zeng, J., Dao, T.M., 2007. Investigation of Influence of Sliding of Rolls over Plate on Continuous Conical Bending. *Proceedings of the 18th IASTED International Conference on Modelling and Simulation, MS 2007*, pp. 527 – 531. May 30 - June 1, Montreal (Quebec, Canada).

Gandhi, A.H., Raval, H.K., 2008. Analytical and empirical modeling of top roller position for three-roller cylindrical bending of plates and its experimental verification. *Journal of Materials Processing Technology*, 197(1-3), 268-278.

Hallquist, J.O., 2005. *LS-DYNA theory manual*, Livermore Software Technology Corporation.

Hua, M., Baines, K., Cole, I.M., 1995. Bending mechanisms, experimental techniques and preliminary tests for the continuous four-roll plate

bending process. *Journal of Materials Processing Technolog*, 48(1-4), 159-172.
Hua, M., Baines, K., Cole, I.M., 1999. Continuous four-roll plate bending: a production process for the manufacture of single seamed tubes of large and medium diameters. *International Journal of Machine Tools and Manufacture*, 39(6), 905-935.
Hua, M., Cole, I.M., Balnes, K., Rao, K.P., 1997. A formulation for determining the single-pass mechanics of the continuous four-roll thin plate bending process. *Journal of Materials Processing Technology*, 67(1-3), 189-194.
Hua, M., Lin, Y.H., 1999a. Effect of strain hardening on the continuous four-roll plate edge bending process. *Journal of Materials Processing Technology*, 89-90, 12-18.
Hua, M., Lin, Y.H., 1999b. Large deflection analysis of elastoplastic plate in steady continuous four-roll bending process. *International Journal of Mechanical Sciences*, 41(12), 1461-1483.
Hua, M., Sansome, D.H., Baines, K., 1995. Mathematical modeling of the internal bending moment at the top roll contact in multi-pass four-roll thin-plate bending. *Journal of Materials Processing Technology*, 52(2-4), 425-459.
Hua, M., Sansome, D.H., Rao, K.P., Balnes, K., 1994. Continuous four-roll plate bending process: Its bending mechanism and influential parameters. *Journal of Materials Processing Technology*, 45(1-4), 181-186. In French.
Lin, Y.H., Hua, M., 2000. Influence of strain hardening on continuous plate roll-bending process. *International Journal of Non-Linear Mechanics*, 35(5), 883-896.
Marroquin, L.R.H., 2002. *Méthodologie de design et de fabrication de la couronne d'une roue Francis*. Mémoire de Maîtrise, Département de Génie Mécanique, Université du Québec à Montréal.
Ramamurti, V., Rao, V.R.S., Sriram, N.S., 1992. Design aspects and parametric study of 3-roll heavy-duty plate-bending machines. *Journal of Materials Processing Technology*, 32(3), 585-598.
Roggendorff, S., Haeusler, J., 1979. Plate bending: three rolls and four rolls compared. *Welding and Metal Fabrication*, v. 47(6), 353-357.
Yang, G., Mori, K.I. Osakada, K., 1994. Determination of forming path in three-roll bending using FEM simulation and fuzzy reasoning. *Journal of Materials Processing Technology*, 45(1-4), 161-166. In Japanese.
Yang M., Shima, S., 1988. Simulation of pyramid type three-roll bending process. *International Journal of Mechanical Sciences*, 30(12), 877-886.
Zeng, J., Liu, Z., Champliaud, H., 2008. FEM dynamic simulation and analysis of the roll-bending process for forming a conical tube. *Journal of Materials Processing Technology*, 198(1-3), 330-343.